

# Study of proton-unbound states in $^{24}\text{Al}$ relevant for the $^{23}\text{Mg}(p, \gamma)$ reaction in novae

E. C. Vyfers,<sup>1</sup> V. Pesudo,<sup>1,2</sup> S. Triambak,<sup>1,\*</sup> P. Adsley,<sup>2,3</sup> B. A. Brown,<sup>4</sup> H. Jivan,<sup>5</sup>  
M. Kamil,<sup>1</sup> D. J. Marin-Lambarri,<sup>1,2,6</sup> R. Neveling,<sup>2</sup> J. C. Nzobadila Ondze,<sup>1</sup>  
P. Papka,<sup>7</sup> L. Pellegrini,<sup>2,5</sup> B. M. Rebeiro,<sup>1</sup> B. Singh,<sup>1</sup> F. D. Smit,<sup>2</sup> and G. F. Steyn<sup>2</sup>

<sup>1</sup>*Department of Physics and Astronomy, University of the Western Cape, P/B X17, Bellville 7535, South Africa*

<sup>2</sup>*iThemba LABS, P.O. Box 722, Somerset West 7129, South Africa*

<sup>3</sup>*Cyclotron Institute and Department of Physics & Astronomy,  
Texas A&M University, College Station, Texas 77843, USA*

<sup>4</sup>*Department of Physics and Astronomy and the Facility for Rare Isotope Beams,  
Michigan State University, East Lansing, Michigan 48824-1321, USA*

<sup>5</sup>*School of Physics, University of the Witwatersrand, Johannesburg 2050, South Africa*

<sup>6</sup>*Instituto de Física, Universidad Nacional Autónoma de México,  
Av. Universidad 3000, Mexico City 04510, Mexico*

<sup>7</sup>*Department of Physics, University of Stellenbosch,  
Private Bag X1, 7602 Matieland, Stellenbosch, South Africa*

(Dated: November 28, 2023)

**Background:** The nucleosynthesis of several proton-rich nuclei is determined by radiative proton-capture reactions on unstable nuclei in nova explosions. One such reaction is  $^{23}\text{Mg}(p, \gamma)^{24}\text{Al}$ , which links the NeNa and MgAl cycles in oxygen-neon (ONe) novae.

**Purpose:** To extract  $^{23}\text{Mg}(p, \gamma)^{24}\text{Al}$  resonance strengths from a study of proton-unbound states in  $^{24}\text{Al}$ , produced via the  $^{24}\text{Mg}(^3\text{He}, t)$  reaction.

**Methods:** A beam of  $^3\text{He}^{2+}$  ions at 50.7 MeV was used to produce the states of interest in  $^{24}\text{Al}$ . Proton-triton angular correlations were measured with a  $K = 600$  QDD magnetic spectrometer and a silicon detector array, located at iThemba LABS, South Africa.

**Results:** We measured the excitation energies of the four lowest proton-unbound states in  $^{24}\text{Al}$  and place lower-limits on  $\Gamma_p/\Gamma$  values for these four states. Together with USD-C shell-model calculations of partial gamma widths, the experimental data are also used to determine resonance strengths for the three lowest  $^{23}\text{Mg}(p, \gamma)^{24}\text{Al}$  resonances.

**Conclusions:** The energy of the dominant first  $^{23}\text{Mg}(p, \gamma)$  resonance is determined to be  $E_r = 481.4 \pm 1.1$  keV, with a resonance strength  $\omega\gamma = 18 \pm 6$  meV.

## I. INTRODUCTION

The  $^{23}\text{Mg}(p, \gamma)^{24}\text{Al}$  reaction is a crucial link between the NeNa and MgAl cycles in oxygen-neon (ONe) novae. Consequently, an accurate determination of this stellar reaction rate is critical for an improved understanding of elemental abundances up to Ca [1, 2]. At peak nova temperatures ( $T_9 = 0.2 - 0.4$ ), the dominant contribution to this process is through the first resonance above the proton threshold in  $^{24}\text{Al}$  (c.f. Fig. 1), at  $E_x = 2345.1 \pm 1.4$  keV [3, 4].

Direct measurements of the  $^{23}\text{Mg}(p, \gamma)$  reaction rate are challenging, primarily because of small cross sections at astrophysically relevant energies and the difficulty in producing intense  $^{23}\text{Mg}$  radioactive ion beams with sufficient purity. As a result, there have been several attempts to determine the  $^{23}\text{Mg}(p, \gamma)$  reaction rate indirectly [5–9], using theoretical estimates of the partial proton and gamma widths of relevant states in  $^{24}\text{Al}$ . For isolated narrow resonances, the resonant contribution for

each level can be obtained from its resonance strength

$$\omega\gamma = \frac{(2J_r + 1) \Gamma_p \Gamma_\gamma}{8 \Gamma}, \quad (1)$$

where  $J_r$  is the spin of the resonance,  $\Gamma_p$  and  $\Gamma_\gamma$  are the partial proton and gamma widths of the resonant state, and  $\Gamma = \Gamma_p + \Gamma_\gamma$  is its total width.

To date, the only direct  $^{23}\text{Mg}(p, \gamma)$  measurement was performed by Erikson *et al.* [10] at the TRIUMF-ISAC facility, where a radioactive  $^{23}\text{Mg}$  ion beam was incident on a hydrogen gas target at the DRAGON recoil spectrometer [11]. Prompt  $\gamma$  rays were detected with an array of bismuth germanate (BGO) scintillators surrounding the target, while the recoils were identified using a combination of ionization chamber and microchannel plate (MCP) detectors located at the focal plane of the spectrometer. However, the experiment was severely affected by a dominant time-varying  $^{23}\text{Na}$  contamination in the beam [10]. This made it difficult to position the resonance at the center of the gas-target and obtain its  $\omega\gamma$  precisely. Nonetheless, the energy of the lowest resonance and its corresponding resonance strength were determined to be  $E_r = 485.7^{+1.3}_{-1.8}$  keV and  $\omega\gamma = 37.8^{+20.5}_{-15.4}$  meV, respectively [10].

\* striambak@uwc.ac.za

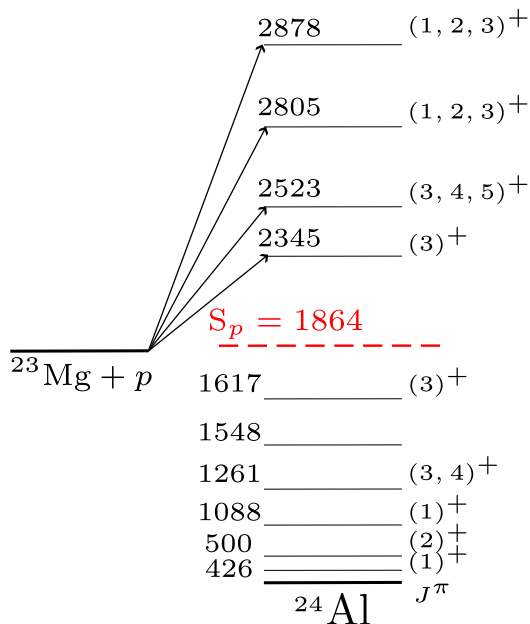


FIG. 1.  $^{23}\text{Mg}(p,\gamma)^{24}\text{Al}$  resonances discussed in this work. Nominal energies (in keV) and spin-parity assignments are from Ref. [3].

Considering the above, in this work we report complementary measurements of proton-unbound states in  $^{24}\text{Al}$ , produced via the  $^{24}\text{Mg}(^3\text{He},t)^{24}\text{Al}$  reaction.

## II. APPARATUS

The experiment was performed at the iThemba LABS cyclotron facility, where a 10 pA, 50.7-MeV dispersion-matched  $^3\text{He}^{2+}$  beam was bombarded on an  $\approx 300 \mu\text{g}/\text{cm}^2$ -thick  $\text{MgF}_2$  target on a carbon backing. The target was located in the scattering chamber of the  $K = 600$  QDD magnetic spectrometer, which was configured in  $0^\circ$  mode, with the beam stop located inside the first dipole magnet [12]. Momentum-analyzed reaction ejectiles were detected in a  $1/4''$ -thick plastic scintillator at the spectrometer focal plane, after passing through two vertical drift chambers (VDCs). The VDCs determined the horizontal and vertical positions of the ejectiles crossing the focal plane, while the plastic scintillator was used for particle identification (PID) purposes, and to generate the data acquisition (DAQ) trigger. The PID plots were generated using the relative time difference between the cyclotron RF and DAQ trigger signals, together with the energy deposited in the scintillator. Fig. 2 shows the PID plot obtained for this experiment, with the triton group explicitly highlighted.

An array of five  $400\text{-}\mu\text{m}$ -thick MMM-type Double-sided Silicon Strip Detectors (DSSDs) called CAKE [13] was used to detect protons from unbound states in  $^{24}\text{Al}$ , in coincidence with triton focal-plane events. These detectors were placed upstream of the target location in a backward-facing lampshade configuration and covered

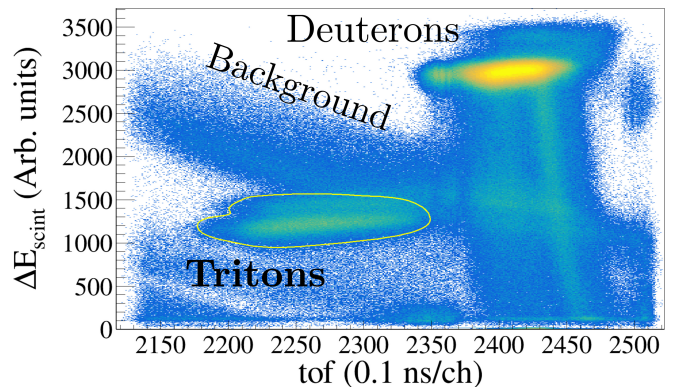


FIG. 2. PID spectrum from energy deposited in the scintillator vs relative time of flight (tof), as discussed in the text.

$\approx 25\%$  of the total solid-angle. Each DSSD comprised 16 ring channels and 8 sector channels. The rings had an angular range of  $\theta_{lab} = 115^\circ - 165^\circ$ , for the array.

## III. DATA ANALYSIS

### III.1. Triton singles

The  $^{24}\text{Mg}(^3\text{He},t)$  singles spectrum, obtained with the appropriate triton PID gate, is shown in Fig. 3. Because the  $^{24}\text{Mg}(^3\text{He},t)$  reaction  $Q$ -value is  $\sim 10$  MeV lower than  $^{25,26}\text{Mg}(^3\text{He},t)$  reactions, one can safely assume negligible contributions from other Mg isotopes in this spectrum. However other contaminant peaks from carbon and oxygen in the target foil cannot be ruled out. To determine such contributions, we took additional ( $^3\text{He},t$ ) data with a  $\text{Li}_2\text{CO}_3$  target, whose spectrum is also shown in Fig. 3. Three contaminant peaks are evident in the region of interest (ROI). We associate these peaks to states in  $^{16}\text{F}$ , produced via the  $^{16}\text{O}(^3\text{He},t)$  reaction.

All triton peaks were fit using a lineshape function defined by a Gaussian distribution convolved with a low-energy exponential tail [14, 15]. Peak centroids ( $\mu_t$ ) and areas ( $A_t$ ) were recorded for later analysis. We next used known excitation energies in  $^{24}\text{Al}$  [3] to perform an *in-situ* energy calibration of the focal-plane spectrum. This was done using a quadratic fit of the form

$$E_{\text{fit}}(i) = a_0 + a_1\mu_t(i) + a_2\mu_t(i)^2. \quad (2)$$

For this procedure, we used the Nuclear Data Sheets [3] to identify calibration peaks within the range  $425 \leq E_x \leq 3328$  keV. The 1.5 and 1.6 MeV states were not included in the analysis, because of possible unresolved doublets in the region [3, 9] and the presence of the contaminant  $^{16}\text{F}$  ground state peak.

In the first trial, the above calibration yielded a poor fit, with reduced chi-squared value,  $\chi^2/\nu = 5.1$ . Further analysis showed that more reasonable agreement ( $\chi^2/\nu = 1.2$ ), with a  $p$  value of 31%, was *only* obtained if we excluded two other points (the 500 and 1261 keV states) from the calibration. The residuals from these

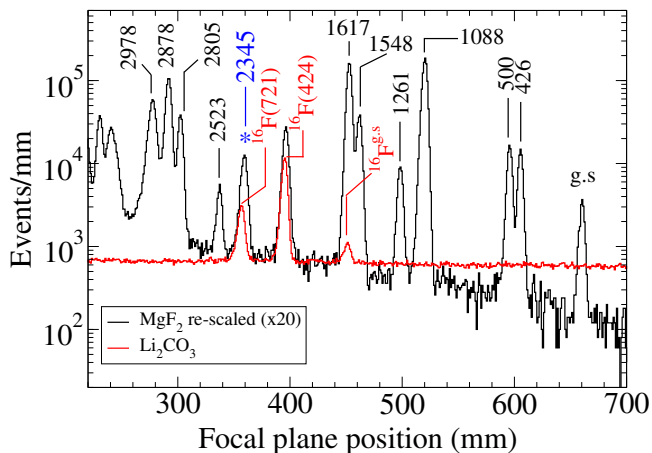


FIG. 3. Triton focal-plane spectra obtained for the  $\text{MgF}_2$  and  $\text{Li}_2\text{CO}_3$  targets. Nominal  $^{24}\text{Al}$  energies are labeled (in keV), with the state corresponding to the first  $^{23}\text{Mg}(p, \gamma)$  resonance marked in blue.

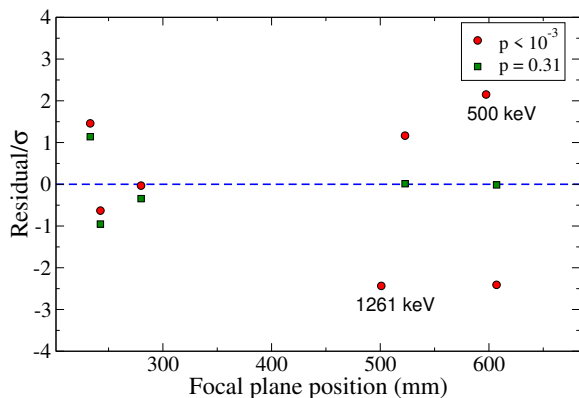


FIG. 4. Residuals for the quadratic fit in Eq. (2), obtained after including (red circles) and excluding (green squares) the 500 and 1261 keV states in the regression analysis.

two fits are shown in Fig. 4. We use the results of this regression analysis to independently determine the excitation energies of observed states in  $^{24}\text{Al}$  that are relevant for the  $^{23}\text{Mg}(p, \gamma)$  reaction rate. These are listed in Table I. For the lowest  $^{23}\text{Mg}(p, \gamma)$  resonance, our calibration yields  $E_x = 2345.5 \pm 1.1$  keV, which is in excellent agreement with a previous  $\gamma$ -ray measurement [3, 4]. Our data do not show explicit evidence of the recently reported state at 2605 keV [16].

The contaminant 721 keV peak from  $^{16}\text{F}$  does not significantly affect our energy determination for 2345 keV state. However it is important that this contamination is corrected for, when the area of the 2345 keV peak is used to determine its corresponding proton branching-ratio. Such a correction is trivial for this case, thanks to the additional high statistics triton peak associated with the 424 keV state in  $^{16}\text{F}$ . Since this peak appears in both spectra (c.f. Fig. 3 around channel number 390), the correction factor was determined from the relative areas of both the contaminant peaks.

TABLE I. Extracted energies for the four lowest  $^{23}\text{Mg}(p, \gamma)$  resonances.

Ref. [3] $E_x$ (keV)	This work	
	$E_x$ (keV)	$E_r$ (keV)
$2345.1 \pm 1.4$	$2345.5 \pm 1.1$	$481.4 \pm 1.1$
$2523 \pm 6$	$2517 \pm 2$	$653 \pm 2$
$2805 \pm 10$	$2790 \pm 2$	$925 \pm 2$
$2878 \pm 6$	$2871 \pm 2$	$1007 \pm 2$

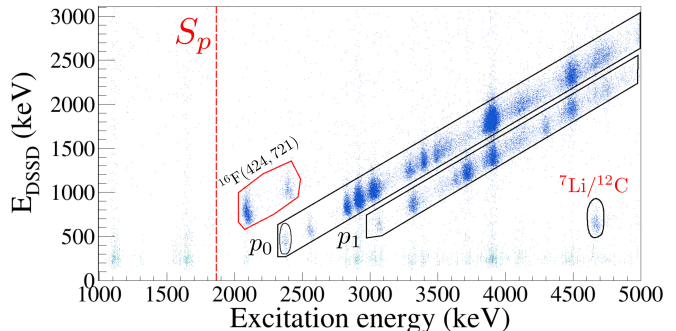


FIG. 5.  $t$ - $p$  coincidence data, with proton groups from states in  $^{24}\text{Al}$  highlighted by diagonal bands. The upper ( $p_0$ ) and lower ( $p_1$ ) bands are from transitions to the ground and first excited states in  $^{23}\text{Mg}$ , respectively. The ellipse around the  $p_0$  proton group is for the lowest  $^{23}\text{Mg}(p, \gamma)^{24}\text{Al}$  resonance.

### III.2. Triton-proton coincidences

As mentioned previously, charged-particle-like events from  $^{24}\text{Mg}(^3\text{He}, t)^{24}\text{Al}^*(p)^{23}\text{Mg}$  were detected using the DSSD array described in Ref. [13]. The energy and timing signals for the array were digitized using CAEN V785 ADCs and V1190A TDCs, respectively. Triton-proton ( $t$ - $p$ ) coincidences were selected by gating on the prompt TDC timing peak, which was around 40 ns wide and further imposing an energy condition on the sector and ring channels (so that they are within 300 keV). The DSSDs were energy calibrated using a  $^{226}\text{Ra}$   $\alpha$ -source at a later time, when the beam was off.

Fig. 5 shows the coincident  $t$ - $p$  energy loci obtained from this experiment. Since each ring of the DSSD array corresponds to a polar angle ( $\theta$ ) with respect to the beam-axis, the proton branching ratios  $B_p(\theta)$  can be determined by gating on the relevant proton groups in Fig. 5, and making use of the formula

$$B_p(\theta) = \frac{N_{tp}(\theta)}{N_t} \frac{1}{\epsilon(\theta)}. \quad (3)$$

Here  $N_{tp}(\theta)$  are the registered  $t$ - $p$  coincidences for a particular ring,  $N_t$  are the corresponding triton singles and  $\epsilon(\theta)$  is the proton detection efficiency of the ring. For states with definite spin and parity, these yields are ex-

pected to follow the simple angular distribution [17]

$$B_p(\theta_{\text{c.m.}}) = \sum_{k=\text{even}} A_k P_k(\cos \theta_{\text{c.m.}}), \quad (4)$$

whose integrated yield gives the total proton branching ratio for each state

$$\frac{\Gamma_p}{\Gamma} = \int_{-1}^1 B_p(\theta_{\text{c.m.}}) d(\cos \theta_{\text{c.m.}}) = A_0. \quad (5)$$

To perform the above analysis, we first determined  $\epsilon(\theta)$  for each active ring of the DSSD array using GEANT4 Monte Carlo simulations. These values were used to obtain an initial set of  $B_p(\theta)$  for the first four  $^{23}\text{Mg}(p,\gamma)^{24}\text{Al}$  resonances. Next, a similar analysis was also performed on the  $^{16}\text{O}(^3\text{He},t)^{16}\text{F}^*(p)$  data, obtained with the  $\text{Li}_2\text{CO}_3$  target. As  $^{16}\text{F}$  is unbound and  $\Gamma_p/\Gamma = 1$  for its observed states [18, 19], this important procedure determined an effective normalization<sup>1</sup> to correct the  $^{24}\text{Al}$  results, which had previously only relied on simulated efficiencies. The renormalized  $t$ - $p$  distributions for the first four proton-unbound states in  $^{24}\text{Al}$  are shown in Fig. 6,<sup>2</sup> with the converged fit results for  $A_0$  and their associated  $\pm 1\sigma$  uncertainties shown in the figure insets. If one assumes Gaussian distributions for these values, it is evident that their coverage probabilities also include disallowed regions of parameter space, with  $\Gamma_p/\Gamma > 1$ . Consequently, we use the fit-results in Fig. 6 to present lower-limits on  $\Gamma_p/\Gamma$  values for all four states. These are listed in Table II.

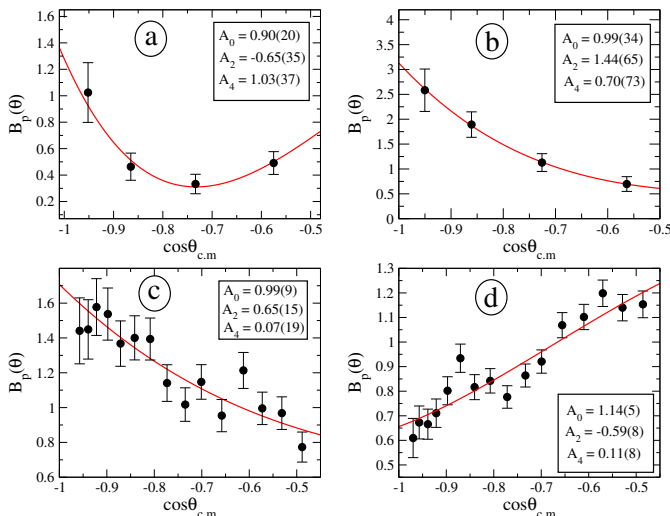


FIG. 6. Legendre polynomial fits to the measured proton-triton angular distributions. The states in  $^{24}\text{Al}$  are labeled by their nominal energies **a**:  $E_x = 2345$  keV, **b**:  $E_x = 2523$  keV, **c**:  $E_x = 2805$  keV and **d**:  $E_x = 2878$  keV.

<sup>1</sup> A weighted mean of the results from the 424 and 721 keV-state data yielded a normalization factor  $\kappa = 1.51 \pm 0.04$ .

<sup>2</sup> As the coincidence data for the 2345 and 2523 keV states were statistics limited, for these cases the angular yield at each bin was obtained by combining data from 4 adjacent strips in the DSSDs.

## IV. RESULTS

TABLE II. Parameters for key  $^{23}\text{Mg}(p,\gamma)^{24}\text{Al}$  resonance reactions.

Assigned $J^\pi$ (from Ref. [6])	$E_r$ (keV)	$\Gamma_p/\Gamma$ <sup>a</sup>	$\Gamma_\gamma$ <sup>b</sup> (meV)	$\omega\gamma$ (meV)
3 <sup>+</sup>	481.4 ± 1.1	≥ 0.64	23	18 ± 6
4 <sup>+</sup>	653 ± 2	≥ 0.55	39	34 ± 11
2 <sup>+</sup>	925 ± 2	≥ 0.87	71	62 ± 18
3 <sup>+</sup>	1007 ± 2	≥ 0.99 <sup>c</sup>	8	...

<sup>a</sup>Unless specified otherwise, lower limits are quoted at the 90% confidence level (CL).

<sup>b</sup>Evaluated using a USD-C [20] shell model calculation.

<sup>c</sup>Quoted at the 99.9% CL.

Although we are unable to quote  $\Gamma_p/\Gamma$  values with sufficient precision, it is still possible to extract meaningful resonance strengths from our data, particularly for the first three states.<sup>3</sup> For this part of the analysis we relied on shell-model-calculated partial gamma widths ( $\Gamma_\gamma$ ), obtained using a recently developed USD-C isospin non-conserving Hamiltonian [20]. Next, we used Monte Carlo simulations to generate Gaussianly distributed random deviates around the measured central  $A_0$  values. Each simulated variable  $A_0^{\text{sim}}$  was used to calculate a corresponding  $\chi^2$  with respect to the measured data points in Fig. 6. Simultaneously, the simulations also determined associated  $\omega\gamma$  values, making use of the relation

$$\left(\frac{\Gamma_p}{\Gamma_\gamma}\right)_{\text{sim}} = \frac{A_0^{\text{sim}}}{1 - A_0^{\text{sim}}}. \quad (6)$$

For each state, the simulated  $\omega\gamma$  that yielded the minimum  $\chi^2$  with respect to our data<sup>4</sup> was accepted as the true value, with its  $\pm 68\%$  CL statistical uncertainties obtained from the values that yield  $\chi^2 = \chi_{\text{min}}^2 + 1$ . Clearly, since  $\omega\gamma$  is proportional to  $\Gamma_\gamma$ , a more realistic uncertainty on the former should include a contribution from the shell model calculation. In order to estimate these uncertainties, we performed similar calculations of level lifetimes in the mirror  $^{24}\text{Na}$  nucleus, which were then compared with experimentally measured values [3]. This comparison is shown in Table. III, based on which we conservatively assign a 30% relative uncertainty to each calculated  $\Gamma_\gamma$  value for  $^{24}\text{Al}$ . These systematic uncertainties from theory are the dominant contributions to the final uncertainties in our extracted  $\omega\gamma$  values, which are listed in Table II.

<sup>3</sup> Since  $\Gamma_p/\Gamma \approx 1$  for the 1007 keV resonance, its  $\omega\gamma$  value is given by its partial gamma width.

<sup>4</sup> Events that yielded  $\Gamma_p/\Gamma_\gamma < 0$  were rejected from the analysis.

TABLE III. Half-lives of states in the mirror  $^{24}\text{Na}$ . A comparison between theory and experiment

Energy <sup>a</sup> (keV)	$J_n^\pi$	$T_{1/2}$ (USD-C) <sup>b</sup> (fs)	$T_{1/2}$ (expt) <sup>a</sup> (fs)
563	$2_1^+$	37000	$35000 \pm 500$
1341	$2_2^+$	350 <sup>c</sup>	$50 \pm 13$
1345	$3_1^+$	30	$26 \pm 8$
1347	$1_2^+$	2200	$4400 \pm 300$
1514	$5_1^+$	28	$27 \pm 6$
1846	$2_3^+$	310	$171 \pm 35$
1886	$3_2^+$	18	$26 \pm 6$
2513	$3_3^+$	23	$10 \pm 5$
2563	$4_2^+$	10	$< 17$
2904	$3_4^+$	38	$35 \pm 8$
2978	$2_4^+$	6.5	$< 17$
3216	$4_3^+$	12	$16 \pm 6$

<sup>a</sup> From Ref. [3].

<sup>b</sup> Effective charges and  $g$ -factors for the  $E2$  and  $M1$  operators were taken from the global sd-shell fit results in Ref. [21].

<sup>c</sup> This state makes a transition to the  $1_1^+$  level at 472 keV [3] with a 95% branch, and is predicted to be  $M1$ -dominated. When corrected for the difference between the theory-predicted (0.53 MeV) and measured (0.87 MeV) transition energy, its calculated half-life is 79 fs.

The final values from Table II were used to evaluate  $^{23}\text{Mg}(p, \gamma)^{24}\text{Al}$  reaction rates with the RatesMC Monte Carlo code described in Refs. [22, 23]. The non-resonant (direct capture) contribution was determined from a polynomial expansion of the  $S$ -factor

$$S(E) \approx S(0) + S'(0)E + \frac{1}{2}S''(0)E^2 \text{ keV b}, \quad (7)$$

whose coefficients were taken from Ref. [6]. The results for individual resonances identified in this work are shown in Fig. 7, with the fractional contribution of each component shown in Fig. 8.

## V. SUMMARY

To summarize, this work reports a study of states in  $^{24}\text{Al}$ , which are important to determine the  $^{23}\text{Mg}(p, \gamma)^{24}\text{Al}$  nuclear reaction rate in ONe novae. Together with shell-model calculations of partial gamma widths, our experimental data are used to determine resonance strengths for the first three  $^{23}\text{Mg}(p, \gamma)$  resonances. Our measured excitation energy for the dominant lowest resonance is in excellent agreement with a previous  $\gamma$ -ray measurement [4]. Making use of the most recent atomic mass data compilation [24], this translates to a resonance

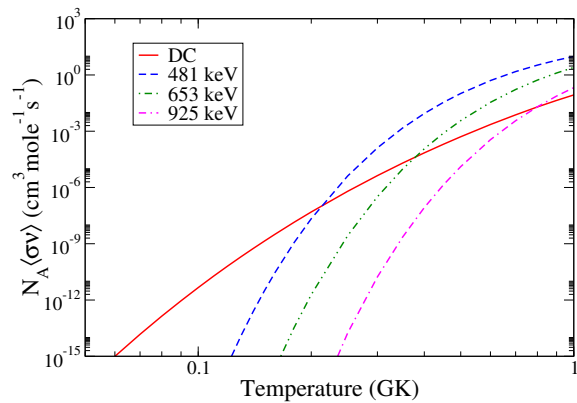


FIG. 7. Median  $^{23}\text{Mg}(p, \gamma)^{24}\text{Al}$  reaction rates obtained from this work. Direct capture (DC) and resonant contributions are shown separately, with the latter evaluated using the results listed in Table II.

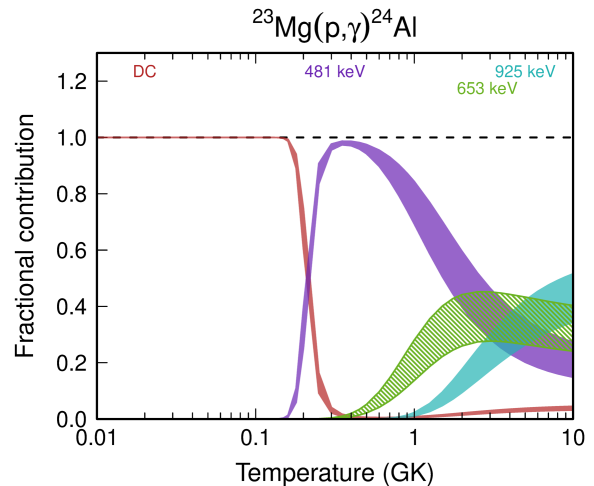


FIG. 8. Fractional contributions of direct capture (DC) and low-lying resonances to the total  $^{23}\text{Mg}(p, \gamma)^{24}\text{Al}$  reaction rate. The uncertainty bands are evaluated using the Monte Carlo prescription described in Ref. [22, 23].

energy  $E_r = 481.4 \pm 1.1$  keV. Our extracted  $\omega\gamma$  value for this resonance is  $18 \pm 6$  meV. These values may be compared with the lower-precision direct-measurement results of Erikson *et al.* [10],  $E_r = 485.7_{-1.8}^{+1.3}$  keV and  $\omega\gamma = 37.8_{-15.4}^{+20.5}$  meV, which relied on extensive Monte Carlo simulations and a joint likelihood analysis to determine their median and  $\pm 68\%$  CL values. The quoted uncertainties in their work were the result of a highly asymmetric joint probability density function (PDF), which showed significant tailing and a double-humped structure for its projected  $\omega\gamma$  probability distribution. Although our extracted  $\omega\gamma$  value is in reasonable agreement with the result reported by Erikson *et al.*, it appears to be more consistent with the left peaked-structure of their PDF for  $\omega\gamma$  (c.f. Fig. 16 in Ref. [10]), which is centered around  $\sim 23$  meV instead.

## ACKNOWLEDGMENTS

We are thankful to Alejandro García for insightful discussions. This work was partially funded by the National Research Foundation (NRF), South Africa under Grant No. 85100. B.A.B acknowledges funding

support from the National Science Foundation, under Grant. No. PHY-2110365. E.C.V thanks the NRF-funded MaNuS/MatSci program at the University of the Western Cape for financial support during the course of his M.Sc.

- 
- [1] K. J. Kelly, C. Iliadis, L. Downen, J. José, and A. Champagne, *Astrophys. J.* **777**, 130 (2013).
- [2] J. José, M. Hernanz, S. Amari, K. Lodders, and E. Zinner, *Astrophys. J.* **612**, 414 (2004).
- [3] M. S. Basunia and A. Chakraborty, *Nuclear Data Sheets* **186**, 3 (2022).
- [4] G. Lotay *et al.*, *Phys. Rev. C* **77**, 042802 (2008).
- [5] R. Wallace and S. E. Woosley, *The Astrophysical Journal Supplement Series* **45**, 389 (1981).
- [6] H. Herndl *et al.*, *Phys. Rev. C* **58**, 1798 (1998).
- [7] M. Wiescher, J. Gorres, F.-K. Thielemann, and H. Ritter, *Astronomy and Astrophysics* **160**, 56 (1986).
- [8] S. Kubono *et al.*, *Nuclear Physics A* **588**, 521 (1995).
- [9] D. W. Visser *et al.*, *Phys. Rev. C* **76** (2007).
- [10] L. Erikson *et al.*, *Phys. Rev. C* **81**, 045808 (2010).
- [11] D. Hutcheon, S. Bishop, L. Buchmann, M. Chatterjee, A. Chen, J. D’Auria, S. Engel, D. Gigliotti, U. Greife, D. Hunter, A. Hussein, C. Jewett, N. Khan, M. Lamey, A. Laird, W. Liu, A. Olin, D. Ottewell, J. Rogers, G. Roy, H. Sprenger, and C. Wrede, *Nucl. Instr. Meth. Phys. Res. A* **498**, 190 (2003).
- [12] R. Neveling, H. Fujita, F. Smit, T. Adachi, G. Berg, E. Buthelezi, J. Carter, J. Conradie, M. Couder, R. Fearick, *et al.*, *Nucl. Instr. Meth. Phys. Res. A* **654**, 29 (2011).
- [13] P. Adsley, R. Neveling, P. Papka, Z. Dyers, J. BrÄmmer, C. Diget, N. Hubbard, K. Li, A. Long, D. Marin-Lambarri, L. Pellegrini, V. Pesudo, L. Pool, F. Smit, and S. Triambak, *JINST* **12**, T02004 (2017).
- [14] S. Triambak, A. García, D. Melconian, M. Mella, and O. Biesel, *Phys. Rev. C* **74**, 054306 (2006).
- [15] M. Kamil, S. Triambak, G. C. Ball, V. Bildstein, A. D. Varela, T. Faestermann, P. E. Garrett, F. G. Moradi, R. Hertenberger, N. Y. Kheswa, N. J. Mukweho, B. M. Rebeiro, and H.-F. Wirth, *Phys. Rev. C* **105**, 055805 (2022).
- [16] R. G. T. Zegers *et al.*, *Phys. Rev. C* **78**, 014314 (2008).
- [17] J. W. Noé, D. P. Balamuth, and R. W. Zurmühle, *Phys. Rev. C* **9**, 132 (1974).
- [18] <https://www.nndc.bnl.gov>.
- [19] D. W. Lee, K. PerÄjÄrvi, J. Powell, J. P. O’Neil, D. M. Moltz, V. Z. Goldberg, and J. Cerny, *Phys. Rev. C* **76**, 024314 (2007).
- [20] A. Magilligan and B. A. Brown, *Phys. Rev. C* **101**, 064312 (2020).
- [21] W. A. Richter, S. Mkhize, and B. A. Brown, *Phys. Rev. C* **78**, 064302 (2008).
- [22] R. Longland, C. Iliadis, A. Champagne, J. R. Newton, C. Ugalde, A. Coc, and R. Fitzgerald, *Nucl. Phys. A* **841**, 1 (2010).
- [23] C. Iliadis, R. Longland, A. Champagne, A. Coc, and R. Fitzgerald, *Nucl. Phys. A* **841**, 31 (2010).
- [24] M. Wang, W. Huang, F. Kondev, G. Audi, and S. Naimi, *Chin. Phys. C* **45**, 030003 (2021).